Toward surface-enhanced Raman scattering using electroless substrate for trace arsenic detection and speciation

Marie Adier, Anne-Marie Jurdyc, Charlotte Hurel, François Goutaland, Jean-Yves Michalon, Alexandre Merlen, Bernard Dussardier, Dominique Vouagner

Journal of Applied Physics

AIP Publishing

Towards Surface-Enhanced Raman Scattering using electroless substrate for trace arsenic detection and speciation

Authors

Marie Adier[1], Anne-Marie Jurdyc[1], Charlotte Hurel[2], François Goutaland[3], Jean-Yves Michalon[3], Alexandre Merlen[4], Bernard Dussardier[2], Dominique Vouagner[1]

Corresponding author : Dominique Vouagner e-mail : dominique.vouagner@univ-lyon1.fr

Affiliations

[1] Institut Lumière Matière (ILM), UMR5306 Université Lyon 1-CNRS, 69622 Villeurbanne, France
[2] Université Côte d'Azur, CNRS, Institut de Physique de Nice (INPHYNI), UMR 7010, Nice, France
[3] Laboratoire Hubert Curien (LabHC), UMR 5516 Université Jean Monnet, 42000 Saint Etienne, France
[4] Institut Matériaux Microélectronique Nanoscience de Provence (IM2NP), UMR 7334, Aix-Marseille Université, Université de Toulon, France

Abstract

Arsenic is one of the most toxic elements present in the environment, especially in water. The World Health Organization (WHO) recommends a maximum concentration of arsenic in drinkable water of 10 µg/L (10 ppb). Sensors implementing Surface Enhanced Raman Scattering (SERS) can detect chemical species at low concentrations. The aim of this study is to compare two kinds of silver-coated SERS substrates for detection and speciation of trace, trivalent and pentavalent, inorganic arsenic compounds. One type of substrates was prepared by a classical thermal evaporation technique, the second type by an electroless process. The thermally evaporated substrates allowed the detection of As(III) only, at a limit of detection (LOD) of approximately 50 mg/L, whereas As(V) could not be detected at any analyte concentration. The electroless substrates allow to differentiate As(III) and As(V) with a LOD 1 µg/L (1 ppb) equal for each valency, below WHO recommendation. The electroless substrates show a very large sensitivity across up to five orders of magnitude in terms of analyte concentration. Although the SERS intensity shows a nonlinear behaviour over this range of concentrations, these preliminary results are encouraging in the framework of the demonstration of trace As SERS sensors in drinkable water.

Keywords

Surface-Enhanced Raman Scattering; Silver Nanofilms; Electroless Deposition; Thermal Evaporation; Trace Detection; Arsenite and Arsenate Detection; Sensor.

Introduction

Arsenic (As) is the 20th most abundant element in the terrestrial crust. Global arsenic pollution has become increasingly important because of its ecotoxicological consequences and especially its harmful effects on human health. Today, millions of people are exposed to elevated doses of As mainly for water, soil and food. Therefore, it is important to monitor water, food and soil with efficient, reliable and high-throughput As detection methods [1,2]. In natural water, As is found as inorganic compounds: arsenite containing trivalent arsenic As(III) and arsenate containing pentavalent arsenic As(V). Nearly 108 countries of the globe are affected by arsenic contamination in groundwater [3]. The biggest scourge is

the pollution of drinkable water causing poisoning of emerging-country populations. It can induce life-threatening diseases such as cancer in the long term. The World Health Organization (WHO) recommendation sets the permissible concentration of As in drinkable water at 10 µg/L (10 ppb or 0.13 µM).

Inorganic As(III) and As(V) relative concentrations depend on the origin and the course of water. As(III) usually predominates in groundwater. When water surfaces or is extracted, contact to air provokes partial oxidation into the other stable valency As(V). Also, rain washing of the soil of polluted industrial sites induces seasonally varying total As concentration as well as the relative As(III) and As(V) concentrations [4]. Industrial accidents may also cause massive river and soil pollution by heavy metals including arsenic, like in the Animas River (Co., USA) in 2015 [5] and in the Orbiel Valley (France) in 2018 [6].

The reactivity and toxicity of As(III) is greater than that of As(V) [7]. Therefore, the quantification of total As concentration is not sufficient to understand and quantify the degree of exposure of populations. Speciation is hence necessary to differentiate the absolute concentrations of As(III) and As(V), respectively, in order to provide reliable information for efficient environment survey. Finally, the monitoring of As total content and relative concentrations among As species is of interest to academic communities in geology and life science [8].

The principal reference methods for speciation of trace As in natural water samples are Induced Coupled Plasma-Mass Spectrometry (ICP-MS) and Atomic Absorption Spectroscopy (AAS, and variants). These techniques are costly and time extensive. They need sample pre-treatment before analysis and are laboratory bound. Hence such techniques are impractical and difficult to implement, for field assays, especially in developing countries [9]. Some field test kits are commercially available. Reactive strips are based on the Gutzeit reaction [10].The reaction between As and strips containing arsine will cause it to stain. The colour of the strip is then compared with a colorimetric quantization scale. Although such kits are inexpensive and allow easy measurements on the field, they have some disadvantages: they are semi-quantitative tests, they form arsine (toxic) and they produce many false positives and false negatives. Also, they do not allow for As(III) and As(V) speciation. Note that Raman spectroscopy would provide speciation, through vibrational fingerprint identification. However, the LOD of As by classical Raman scattering is as high as 23 g/L [11]. Electrochemical sensors are promising products: their high sensitivity allows easy detection of As, down to 1µg/L. Research and development on this technology is intense [12,13,14]. However, the presence of other metal ions in the water can cause interferences and distortion of the results, and the presence of an operator is necessary for the measurement.

Surface Enhanced Raman Scattering (SERS) is a promising technique for the detection of biocomponents in water, at trace level [15]. A fewer works report on the detection of inorganic compounds, such as arsenic or metals, though many applications are foreseen. Characterizing of molecules by SERS is commonly performed using noble metal nanoparticles like gold, silver (Ag) and copper. Under excitation by an external electromagnetic field at an appropriate wavelength, metal nanostructures produce localized surface plasmon resonance (LSPR) defined as the collective oscillation of free electrons of metal [16]. The two well-known mechanisms to account for the origin of SERS are the electromagnetic (EM) and chemical or charge transfer (CT) mechanisms. Nanostructured Ag is a very sensitive material for SERS detection of As. The first detection of As by SERS was reported in 1988 by Greaves and Griffith, with a high concentration in As(V) (100 g/L). They used a suspension of Ag colloids as a SERS "volume" substrate [17]. The review of Hao et al. describes SERS properties of many chemically processed Ag SERS substrates: mirror reaction, electroless process, Ag colloids, Ag nano wires by a two-phase interfacial self-assembly, etc. [11]. The best Ag substrate in the scientific literature is an Ag nanoporous film doped with γ-Fe_2O_3 nanosheet and developed by Liu and al. [18]. Arsenic is adsorbed on a Ag-based hybrid nanocomposite surface. The LOD of this substrate is 1ppb for As(V) and 10 ppb for As(III), below or near WHO recommendation [18]. In the case of electroless substrate, Hao et al studied As(V) only, and have detected it down to 5 µg/L, 5 times higher that WHO recommendation [19]. However, both proposed manufacturing processes require several steps using basic compounds toxic to the environment.

Our aim is to study and demonstrate SERS substrates dedicated to heavy metal oxides, like As(III) and As(V) that are efficient, sensitive (below WHO recommendation), supporting a large concentration range over several decades. They shall preferably be low-cost, versatile, easily attached to transductors like glass substrates (flat or cylindrical, e.g. fiber cladding), as well as corrugated substrates [16]. Here we report on the study and comparison of two types of SERS substrates for As detection, elaborated by thermal evaporation and by electroless process, respectively. Both manufacturing processes are fast and require few steps. The starting compounds have a low environmental toxicity: this is a benefit for detection measurements in natural as well as potable water. Physical deposition, such as thermal evaporation, is in principle more reproducible and repeatable than chemical deposition processes. The former requires a more expensive facility, whereas the latter needs inexpensive, basic chemistry lab equipment. In this work, we compare both processes in terms of sensitivity and LOD.

After manufacture, we have characterized the deposited layers by AFM and optical extinction measurements. Then the SERS response of methylene blue (MB) solutions were characterized. MB is a well-known probe molecule used to evaluate the SERS effect [20]. This molecule belongs to the dyes family characterized by a large value of polarizability leading to huge SERS signal [21]. We conducted tests for detection and speciation of As(III) and As(V), in separate dilute solutions, over a wide range of concentrations. To the best of our knowledge, it is the first time that As-detection by SERS is performed on an Ag substrate made by a physical process. The results are discussed in the light of the experimental characteristics, such as plasmonic and structural properties including surface roughness. The variation of the SERS intensity relative to As(III) and As(V) signals as a function of analyte dilutions is also discussed as well as the adsorption of the arsenic mechanisms on the silver surface.

Experimental

-Silver SERS substrates elaboration

Two kinds of silver SERS layers were elaborated: electroless-deposited and thermally evaporated layers. The glass substrate slides were washed in a piranha solution (1/3 H_2O_2; 2/3 H_2SO_4) for 20 minutes and rinsed successively in an acetone bath for 5 minutes and an ethanol bath for 5 minutes. For the electroless process, the glass slides were immersed in a $SnCl_2$ solution (concentration C=1g/L) for 15 minutes to sensitize the glass surface for silver deposition. The glass slides are then briefly plunged into a $AgNO_3$ solution. Sn^{2+} ions react with Ag^+ ions to produce Ag^0, that will serve as catalyst for the electroless reaction. The electroless reaction is performed by putting the slides in the Tollen's reagent bath during 30 minutes by maintaining a vigorous agitation of the solution. The used Tollen's reagent was a silver nitride ($AgNO_3$) solution (C=0.03 mol/L) in ammonia medium with the pH adjusted to 8.8. The thickness of the electroless layer was 98 ± 5 nm, as measured by mechanical profilometry. For the thermal evaporation process, the layer deposition was performed in a homemade vacuum chamber at a pressure of 6.10^{-6}mbar. The initial current across the Ag source was 110 A, then lowered to 105 A. The silver layer thickness was controlled in situ using a quartz crystal scintillator. The initial growth speed was 2.0 nm/s, then 1.5 nm/s. The layer final thickness was 90 ± 5 nm.

- Structural and optical characterization of the Ag SERS substrates

Roughness measurements were performed with a Bruker Dektak XT profilometer. The window scanning was 1 mm for each measurement. The average roughness (R_a) was measured. AFM was performed in air, using an MFP-3D Asylum Research Oxford AFM. Images were recorded using a silicon cantilever. The grain size was determined with Gwyddion© software [22]. The roughness was estimated with the Dektak XT profilometer software.

Transmission extinction spectra were measured through the glass slides and the deposited layers with a UV-Visible-Near Infrared Perkin Elmer spectrophotometer. The measured light intensity transmitted though the samples was compared with that through a blank glass slide as a reference. The spectral range extends from 300 to 1000 nm with 2-nm resolution.

- Analytes elaboration for SERS measurements

Methylene blue (MB) solutions were prepared from MB powder and distilled water. The parent solution (1,00 ±0,02).10^{-1} mol/L was made with 3,2 g of MB powder in 100 mL of distilled water. The other solutions were prepared from successive dilutions of the parent solution, with a wide range of MB concentrations from 3,19.10^{-6} g/L to 3,19 g/L. The pH of the solutions was between 6 and 6.5. The precision in the concentration of the diluted MB solutions is estimated to be 1 %.

The arsenic solutions were elaborated from standard arsenic solutions used for the calibration of mass spectrometry measurements. The As(III) standard solution had a concentration of 1000 ppm (1 g/L) and traces of NaOH. The As(V) standard solution had a concentration of 1000 ppm (1 g/L) and 2 % HNO_3. NaOH and HNO_3 are valency stabilizers in the respective standard solutions. NaOH and HNO_3 do not interact with As detection by SERS [23][24]. The concentration range of the diluted solutions was set between 0.1 g/L and 1 µg/L; the latter is below the WHO recommendation (10 µg/L). TABLE I lists the concentrations and pH of the As(III) and As(V) solutions. The precision in the concentration of the diluted As-solutions is estimated between 0.3 % and 1 %. Note that the pH of As(III) solutions below the concentration 10^{-4} g/L is less than 7. It is a consequence of the well-known acidification of water by the absorption of atmospheric CO_2.

TABLE I : Concentrations and pH of the diluted As(III) and As(V) solutions in water, respectively. The As(III) solutions contain traces of NaOH, whereas the As(V) solutions contain traces of HNO_3.

As(III) solutions		As(V) solutions	
Concentration (g/L)	pH	Concentration (g/L)	pH
10^{-1}	11.9	10^{-1}	1.4
10^{-2}	10.9	10^{-2}	2.1
10^{-3}	9.1	10^{-3}	3.0
10^{-4}	6.1	10^{-4}	3.5
10^{-5}	6.5	10^{-5}	4.0
10^{-6}	5.7	10^{-6}	4.5

- Classical Raman and SERS measurements

Raman spectra were obtained with a fully confocal DXR ThermoFisher spectrophotometer operating at an excitation wavelength of 780 nm delivered by a frequency-stabilized single mode diode laser. A confocal 50-µm pinhole was set to allow measurements with a 2 µm depth resolution in an optically transparent sample. The laser power was set at 14 mW, corresponding to 9 mW incident power on the sample. The microscope magnification was x10 (Numerical Aperture = 0.25), leading to a laser spot diameter estimated at 4 µm. The estimated power density on the sample was ~ 0.7 mW/µm^2. A high-resolution grating provided a spectral resolution of 3 cm^{-1}. The Rayleigh peak was cut by an edge filter included into the setup. Each measurement consisted of 20 exposures of 3 sec duration each. The background noise of the SERS measurements was less than 10 counts per second (cps). The limit of detection (LOD) was estimated from the crossing of the extrapolation of the SERS intensity vs concentration curves and the 10-cps level.

SERS measurements of MB and arsenic (the analytes) were performed on the SERS substrate samples, at 780 nm excitation, using the diluted solutions. They were carried out as follows : a droplet of analyte solution was deposited on the sample surface. The laser beam was focused on the interface between the sample surface and the drop. The repeatability conditions of the measurement were checked by performing the detection of analytes five times on the same substrates and the same drop of analytes, without changing any of the measurement parameters, in a short period of 20 minutes. This study was performed for all solutions of analytes and by the same experimenter. The reproducibility conditions of the measurement were checked by performing the measurement for the same dilutions

of arsenic on three substrates of different series, with the same spectrophotometer and approximately the same volume of solution drop. Comparisons of measurements taken from different spots of every sample dit not show noticeable modification between SERS spectra. Note that the substrates were stored in air, and that all SERS measurements were performed several days after the fabrication. Surprisingly, no significative shift nor lowering of signal was observed.

Results and discussion

Characterization of the silver SERS substrates

Surface imaging of the silver SERS layers by atomic force microscopy (AFM)

The surface AFM images are shown on Figure 1 for a selected sample of both types of substrates. The average roughness (R_a) is estimated by mechanical profilometry. The arithmetic average of the absolute values of the deviations, between peaks and troughs is calculated. *Ra* measures the distance between this average and the "center line". It clearly appears on Fig. 1(a) that the electroless-deposited silver layer is granular with inhomogeneous grain shapes and size. The grain or nanoparticle size is (101±10) nm and the average roughness (R_a) is (21±2) nm. On the opposite, the thermally evaporated silver layer has a more continuous and less structured appearance and is characterized by a low roughness value equal to (3±0,5) nm (Fig. 1(b).

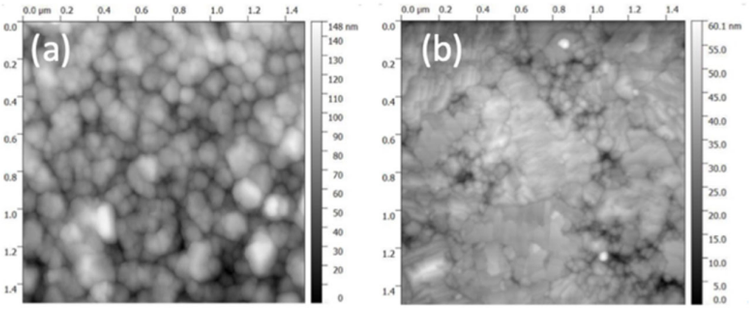

Figure 1 : AFM images: (a) Electroless-deposited silver layer; (b) Thermally evaporated layer. The total field of view is 1.5 µm x 1.5 µm. The thickness is coded on a grey scale, from black (0 nm) to white (148 nm (a) and 60.1 nm (b), respectively).

Optical extinction characterization of the silver SERS layers

Extinction spectra represented by the optical density (OD) versus wavelength are depicted Figure 2 for both kinds of SERS substrates. Both spectra show a general trend, that is an increasing optical density when wavelength increases. This is due to the wavelength sensitive reflectivity of silver films. However, one notices a large band with a maximum near 560 nm recorded for SERS substrates elaborated with an electroless-deposited silver layer (Fig. 2(a)). Usually, the LSPR band maximum of spherical monodisperse silver nanoparticles is located near 420 nm [25]. Nevertheless, a shift can be explained by different phenomena. The first hypothesis is due to the inhomogeneity of the geometry of nanoparticles deposit. This shift of the maximum is most likely due to the nanoparticles shape that is not spherical as shown by the AFM image of Figure 1(a). Mock et al explain that there is a shift of the plasmon band position from 420 nm to 700nm, attributed to the shape and size of nanoparticles, that agrees with our results [25]. Moreover, an inhomogeneous nanoparticle shape as observed in Figure 1(a) can also explain the silver plasmon band enlargement. Another hypothesis is that the silver films surface may have been oxidized into Ag_2O between the elaboration and the absorption measurement. According to Chatterjee, a red shift in the plasmon band may be due to the presence of oxide on the silver surface [26]. They obtained an LSPR for oxide nanoparticles between 550 and 700 nm. Another cause may be a result from pollution by sulphur from ambient air. A thin layer of sulphur (Ag_2S) can shift the LSPR by around 100 nm [27]. The last hypothesis is the presence of a strong coupling between Ag nanostructures [28,29]. This phenomenon can shift the LSPR by around 60 nm [30]. This hypothesis may

explain that two bands are observed: the one around 380 nm attributed to quadrupole contributions, and the one around 560 nm to dipole contributions, respectively [31]. Nevertheless, the observed red shift would contribute to the improvement of the plasmon excitation, and hence Raman exaltation and SERS, because the excitation wavelength (780 nm) is near the extinction band.

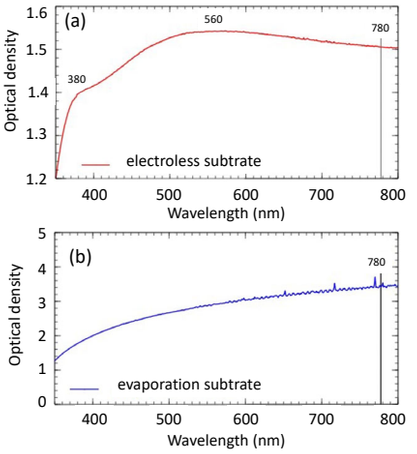

Figure 2 : Optical density spectra of the SERS substrates with (a) Electroless-deposited silver layer, (b) Thermally evaporated silver layer. 780 nm is the excitation wavelength

Conversely, no resonance is observed from the substrate made by thermal evaporation (Figure 2(b)). Instead of this, absorption increases monotonously throughout the visible range. This observation can be explained by several hypotheses. Since the measurements were carried out without an integrating sphere, the transmission spectrum obtained is in fact a reflectance spectrum [32]. For thicknesses of the order of 90 nm deposited by evaporation, the percolation threshold is exceeded, and the film is semi-continuous (Figure 1 (b)). With this type of film, it is no longer possible to use optical absorption to measure the plasmonic response. According to Seal et al, in semi-continuous films obtained after the percolation threshold, there may be the coexistence of localized and delocalized plasmons. To demonstrate this coexistence, these authors used SNOM (Scanning Near-field Optical Microscopy) [33]. These techniques are difficult to implement because it is necessary to have ordered structural substrates to be able to interpret the results [34]. Because localized plasmons are necessary to obtain a high SERS sensitivity, it is critical to obtain localized plasmons by manufacturing thin films [16]. We have thermally evaporated a 5-nm thick Ag layer. On this we have observed an OD maximum at around 420 nm (result not shown here), attributed to LSPR. This value is in accordance with the literature for Ag nanostructures of circular shape [25,35]. However, this thin Ag coating peeled off when a droplet of As solution was deposited on it, due to surface tension and low adhesion power of Ag on glass. An adhesive undercoating would have overcome this, at the risk of generating parasitic Raman bands, that would have been difficult to discriminate from the signal from arsenic. That is why the thermal-evaporated substrates with low silver thickness are not suitable for As detection by SERS. The study of possible effects of adhesive undercoating on SERS is out of the scope of this work. In the following, we report studies on the thicker evaporated substrates without adhesive undercoating.

SERS efficiency evaluation of the substrates on methylene blue

We have estimated the LOD of MB and used it as a criterion to evaluate and compare the SERS efficiency of both types of substrates. Figures 3(a) and 3(b) show SERS spectra of a MB solution at $3{,}19.10^{-2}$ g/L recorded with both types of substrates. The most intense characteristic peaks of MB located at around 445 cm^{-1} and 1625 cm^{-1} are clearly visible. These bands are assigned to C-N-C skeletal bending vibrations and C-C stretching, respectively [36,37]. No MB band is detected for this diluted solution when MB is deposited directly on a bare glass substrate. This indicates that both types of substrates are SERS-efficient. Then, the SERS detection capacity of MB on both substrate types has been

characterized using the prepared diluted MB solutions, over five orders of magnitudes in concentration. The spectra were all identical, except for the decreasing of signal strength and signal-to-noise ratio when the concentration decreases. In Figure 3(c), the intensity of the 1625 cm^{-1} band is plotted against the MB concentration on both types of substrates. Note that the log-log representation is more appropriate because of the large difference between the signal levels from both substrates. The LOD for the electroless substrate is estimated near 10^{-6} g/L. It is around 10^{-2} g/L for the thermally evaporated one (Figure 3(d)), that is four orders of magnitude higher than for the electroless substrate. Note that the SERS signal from the electroless substrates is much higher than that from the thermally evaporated one. It can be concluded that the electroless SERS substrate has a better SERS efficiency than the substrate made by evaporation.

In the literature, it is shown that the rougher the surface, the higher is the SERS performance. This higher SERS amplification is due to the increase of the surface area with roughness. On one hand, the electromagnetic wave is intensified on the rough edges [38,39,40]. In addition, large scale roughness (10-200 nm) promotes the molecule adsorption on the substrate, and hence promotes the EM SERS mechanism [41]. Moreover, when molecules are captured by, and adsorbed to plasmonic metal surfaces through chemical bonds, they can easily be excited by plasmons to generate SERS signals of their molecular fingerprints [21].

For all the concentrations studied here, no band shift was observed on the SERS spectra. In the literature, it has been reported that the molecular adsorption may be influenced by the concentration of solutions and could play a role on the Raman shift and on the intensities of the observed SERS peaks [36,37,42]. We conclude that the adsorption of MB on both substrate types may not be influenced by the concentration over the whole range studied here.

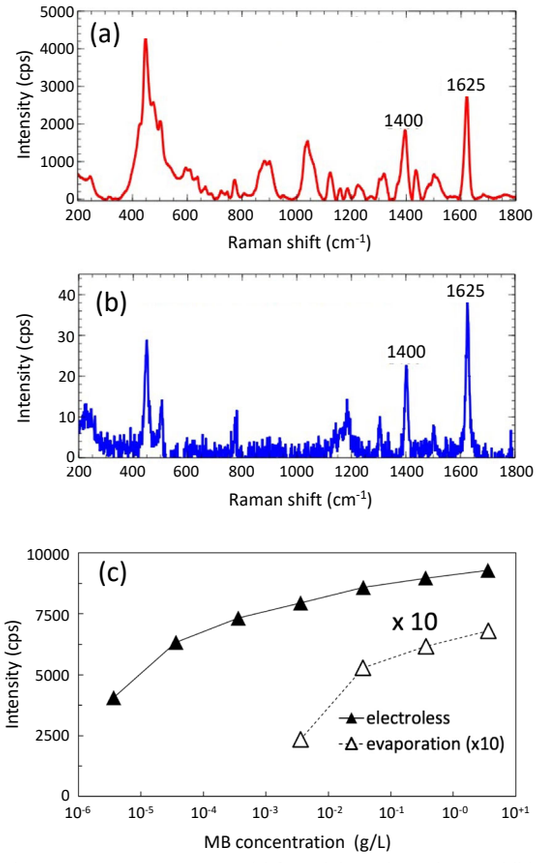

Figure 3 : SERS spectra of MB (concentration 3.19x10-2 g/L) from (a) an electroless and (b) thermally evaporated substrates (spectra without baseline). (c) Peak intensity of the 1625-cm-1 peak versus MB dilutions for both substrate types, in lin-log scales.

On both types of substrates, the intensity of the 1625 cm^{-1} band increases monotonously with increasing concentration. An apparent saturation (in the semilog graph) is observed at the higher concentrations, with a more important change of sensitivity around 10^{-3} g/L on the electroless substrates and around 5.10^{-2} g/L on the thermally evaporated substrates (Fig. 3(c)). In some cases, SERS bands intensity versus concentration laws can be established, such as linear, power or exponential laws, but usually on a very limited concentration range, typically less than few orders of magnitude [43]. Further, these laws are often used for engineering purposes rather than physical and chemical interpretation of the SERS mechanisms. There are limitations of these laws towards higher concentrations since deviations due to saturation or geometrical effects cannot be avoided and are highly dependent on experimental parameters. Proposing a law over such a large range of concentrations is out of the scope of our study because of the many possible mechanisms involved. Further investigations are needed to fully interpret our results on their whole.

However, the intensity curve of MB in Figure 3(c), is separated into two zones; this is much more visible on the electroless substrate. This behaviour change may be due to the influence of the MB molecular adsorption geometry, with adsorption parallel (resp. perpendicular) to the silver surface at low (resp. high) concentrations [44]. It is well documented that the adsorption of MB molecules at high concentration induces the growth of H-aggregates (through π-π interactions), which induces steric hindrance. Thus the MB aggregates are oriented not parallel to the surface, or even perpendicular to it [45].

Arsenic detection by SERS

The As(III) and As(V) detection efficiency was evaluated for both types of SERS substrates in terms of LOD. This study has been done for a wide range of concentrations between 10^{-6} and 10^{-1} g/L for each species. Few literature studies have been conducted over such a wide concentration range for the study of As(V) and As(III).

- As(III) detection

The SERS spectra of an As(III) solution (10^{-1} g/L) recorded on both types of substrates are shown in Figures 4(a) and 4(b). They show that both are SERS-sensitive for As(III) detection. The characteristic peaks of As(III) are visible: the peaks in the range 730-770 cm^{-1} and 440 cm^{-1} are assigned to the symmetric As-O and As-OH stretching vibrations, respectively. The most intense peak near 750 cm^{-1} is used in the literature to plot As(III) SERS signal versus its concentrations [11].

The intensity of the peak from 730 or 770 cm^{-1} is plotted versus As(III) dilutions on Figure 4(c) for both substrate types. The As(III) detection threshold (LOD) is 10^{-6} g/L using the electroless substrate, that is much lower than that measured with the thermally evaporated substrate (~5.10^{-3} g/L). Hence, As(III) can be detected below the WHO limit (10 µg/L or 10^{-5} g/L) using the electroless substrates. On the curve relating to the electroless substrate, figure 4(c), a change in behavior is observed around C=5.10^{-4} g/L. There is no observable total saturation over the entire concentration range studied, even at high concentrations. In the insert of Figure 4(c), a rapid increase in the SERS signal is observed at very low concentrations, followed by a decrease in the slope from the concentration 10^{-4} g/L and above.

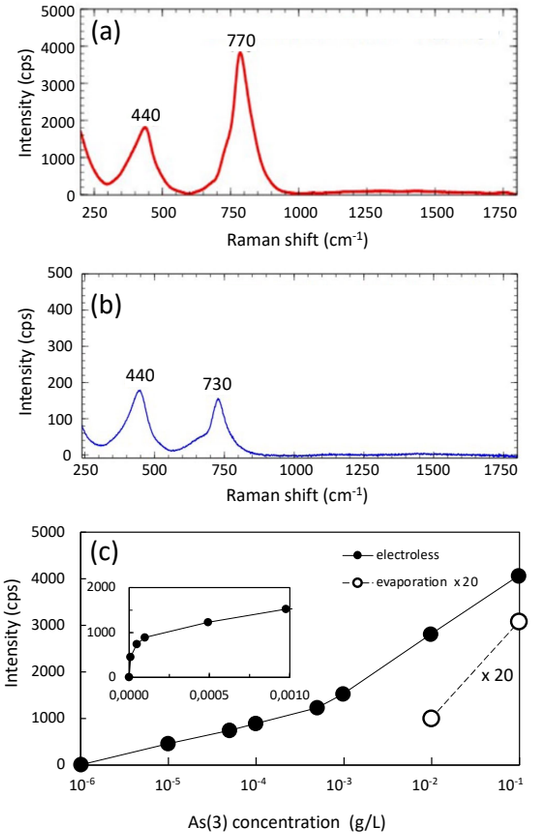

Figure 4 : SERS spectra of a 0.1 g/L solution of As(III) from (a) an electroless substrate and (b) a thermally evaporated substrate. (c) SERS intensity of the peak around 730-770cm-1 versus As(III) concentration for both substrate types. Data for the thermally evaporated substrate are multiplied by 20. Inset of (c): SERS intensity in linear-linear scales, for concentrations below 1 mg/L

- As(V) detection

Figures 5(a) and 5(b) present SERS spectra of an As(V) solution (10^{-1} g/L) recorded for both kinds of SERS substrates, respectively. In our experimental configuration, the signal with the thermally evaporated substrate produced only a noisy background (Fig. 5(b) and no plot of the signal vs concentration was possible. The characteristic peaks of As (5) are visible only in the case of the electroless substrate (figure 5(a)). The 830-cm^{-1} peak is assigned to the symmetric As-O stretching vibration while the other minor peak at 570 cm^{-1} is attributed to a superposition of stretching modes of As-OH [11,46]. Figure 5(c) shows the plot of the 830-cm^{-1} peak of As(V) intensity against concentration using the electroless substrate. The signal increases monotonously and no saturation is observed on the concentration range under study. The As(V) LOD is 10^{-6} g/L, much below the WHO recommendation (10^{-5} g/L). The insert of figure 5c) shows a very fast growth of the signal at very low concentrations, followed by a levering of the slope around 10^{-4} g/L. The behaviour is-qualitatively similar to that of As(III) on the electroless substrate (insert of fig 4(c)).

It is interesting to compare the signal levels between As(III) and As(V) on the electroless substrate (Figures 4 and 5). Though the experimental conditions were identical for both arsenic valencies, the signal observed for As(III) is more than one order of magnitude higher than that from As(V). This could be attributed to the better adsorptivity of As(III) than that of As(V) onto the substrate. Another hypothesis to explain this difference is the possible presence of oxide or sulphur on the surface of the substrate. Indeed, As(III) has a better affinity with sulphur deposited on silver surface [47]. This would

be an additional interpretation of the fact that As(III) for high concentrations have a stronger SERS signal than As(V). This would also agree with one of the hypotheses that explains the red shift of the plasmon resonance.

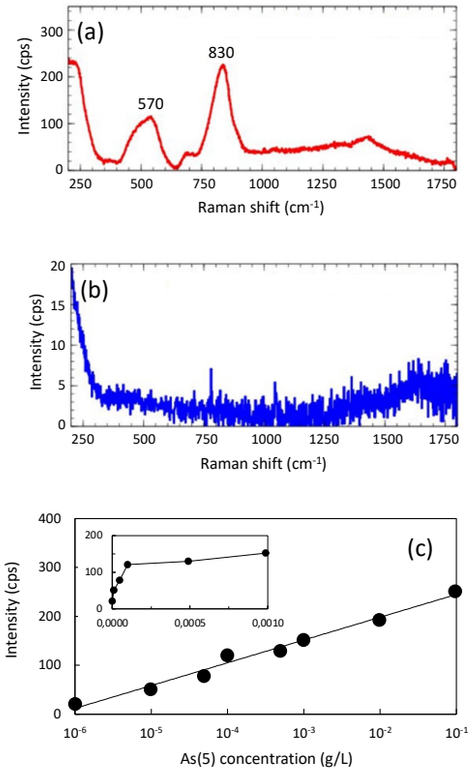

Figure 5 : SERS spectra of a 0.1 g/L solution of As(V) with (a) an electroless substrate and (b) a thermally evaporated substrate. (c) SERS intensity of the 830-cm^{-1} peak versus As(V) concentration, in log scale, on the electroless substrate. Inset of (c): SERS intensity in linear-linear scales, for concentrations below 1 mg/L. The thermally evaporated substrate was not sensitive to As(V).

This rapid increase in the SERS signal, from very low concentrations, for As(III) and As(V), shows the acute sensitivity of the electroless nanostructured silver substrate for the detection of this pollutant in its two ionic forms at the trace state. This sensitivity decreases with increasing concentration without saturation of the SERS signal being reached. This highlights the ability of the substrate to detect arsenic in the As(III) and As(V) forms in a wide range of concentrations. Finally, the change in behavior observed for the chemical species As(III) towards 5.10^{-3} g/L shows that the results are very sensitive to the adsorptive properties of chemical species on the SERS surface. This change is tentitatively correlated to the pH of the solutions (see TABLE I). Indeed, the concentration of As(III) solutions as a function of pH in and the associated speciation diagram are shown in Figures 6(a) and 6(c), respectively [48; supplementary information]. It is seen that when the pH changes induce a modification of the ionic form of detected As(III). H_3AsO_3 is the main ionic form at $C < 10^{-3}$ g/L and pH < 9, whereas $H_2AsO_3^-$ is the main one for $C > 10^{-3}$ g/L and pH > 9. The lack of behavioral change for the As(V) form is consistent with the existence of a single ionic form ($H_2AsO_4^-$) over all the concentration and pH ranges studied [48].

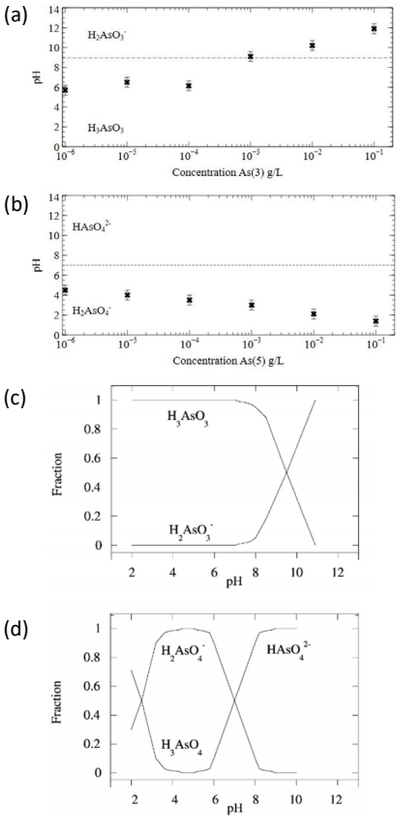

Figure 6 : pH versus concentration for (a) As(III) and (b) As(V). Data are extracted from As speciation diagram for As(III) (c) and (d) As(V) (from Supplementary information, fig S8 of ref [48]).

Our study applies to a very large range of concentrations, from 10^{-1} to 10^{-6} g/L (5 decades). Other observations in the literature apply to much more limited ranged of concentrations, For example, 0.18-180 ppb (3 decades) [46] or 1-13 mg/kg (in field soil), ~1.5 decade) 49]. Therefore, it is difficult to compare our results on such a larger concentration range, with already published report on the detection of arsenic using SERS. To be able to interpret the behavior of the signal according to the concentrations of As(III) and As(V) on the electroless substrates, it would be necessary to make an in-depth study on, on the one hand, the fine structure of the silver layer. , and on the other hand chemical species present on the surface. This requires many multidisciplinary investigations, and their effect on the interactions between arsenic species and the pH-sensitive hydrophilic/hydrophobic character of the surface.

Conclusion

In this study, we have compared the sensitivity and the LOD of arsenite and arsenate over a very large range of concentrations (10^{-6}-10^{-1} g/L) on two types of SERS substrates. The substrates were made by an electroless method and by a thermal evaporation method, respectively. The electroless substrate has a granular nanostructure and a high roughness (21 nm) while the other has a more continuous layer structure and a lower roughness (3 nm): this difference has a great influence on the SERS response. On the thermally evaporated substrates, the As(III) LOD was ~ 5.10^{-3} g/L (5 ppm) and no As(V) was detected. The electroless substrates have a lower LOD =10^{-6} g/L (1 ppb) for both As(III) and As(V). This is an order of magnitude less than the WHO recommendation of total As content in drinkable water. To our

knowledge, the lowest As(III) LOD for silver nanofilm was 10^{-5} g/L (10 ppb). The adsorption efficiency of As(III) is an order of magnitude higher than that of As(V) on the electroless substrates. This ratio could be explained by the presence of parasitic compounds on the silver surface (oxides or sulphurs) of the electroless substrate. These surface species may also explain the redshift of the plasmon band. These hypotheses necessitate further investigations. This relationship on such a wide range of concentrations would potentially serve as a calibration over five orders of magnitude in arsenic concentration, to help developing a sensor for trace arsenic as well as for food industry (medium concentrations) and soils (acceptable threshold ~7.10^{-3} g/kg (7 ppm) [49], as well as production of medicine or materials containing arsenic (concentrations > 10^{-3} g/L). Finally, although the electroless substrates were elaborated using basic and rather environmentally friendly chemicals, and laboratory equipements, it allowed a better detection of As than the physically deposited substrates. This would give a better potential to electroless technique for the demonstration and development of field sensors for the detection of Arsenic.

Acknowledgements

- European Regional Development Fund (FEDER)-CNRS Université Côte d'Azur (OPTIMAL platform at INPHYNI)
- Université Côte d'Azur ,«Space, Environment, Risk and Resilience» Academy of Excellence
- GIS GRIFON, Groupement d'Interêt Scientifique « GRoupement d'Initiatives pour les Fibres Optiques Nouvelles », CNRS, France
- Wolfgang Doeblin Federation of Research (UCA Nice, CNRS)-France
- PlateForme Chimie-Physique (PFCP), Lyon, France (Lionel Clouzeau)

Author Declarations

The authors have no conflicts to disclose.

Data Availability

The data that support the findings of this study are available within the article.

References

1 S. J. Flora, «Arsenic: chemistry, occurrence, and exposure,» in *Handbook of Arsenic Toxicology*, Elsevier Inc., 2015, pp. 1-49.

[2] M. Singh and M. del Valle, "Arsenic biosensors: Challenges and opportunities for high-throughput detection," in *Handbook of Arsenic Toxicology*, Elsevier Inc., 2015, pp. 575-588.

3 E. Shaji, M. Santosh, K.V. Sarath, Pranav Prakash, V. Deepchand, and B.V. Divya, "Arsenic contamination of groundwater: A global synopsis with focus on the Indian Peninsula," Geoscience Frontiers 12(3), 101079 (18 pages) (2021).

[4] A. Chatterjee, D. Das and D. Chakraborti, «A study of ground water contamination by arsenic in the residential area of Behala, Calcutta, due to industrial pollution,» *Environmental Pollution* 80(1), 57-65 (1993).

[5] E. Morgan, «Durango copes with 'orange nastiness' of toxic sludge river pollution,» *The Guardian,* 10 August 2015.

[6] M. Dundas, V. Dekimpe, J. Lacharnay, J. Guggenheim and M.-C. Ide, «Arsenic pollution: A toxic legacy of France's gold rush,» 15 Febuary 2019. Available: https://www.france24.com/en/20190216-down-earth-france-pollution-gold-mine-arsenic-toxic-waste-salsigne-aude. [Access 27 July 2022].

[7] B. A. Fowler and S. Flora, «Arsenical kidney toxicity,» in *Handbook of Arsenic Toxicology*, A. Press, Ed., Oxford, Elsevier, 2015, pp. 349-361.

[8] A. Barats, G. Feraud, C. Potot, V. Philippini and Y. Travi, «Alpine/Mediterranean Var River watershed (France),» *Science of the Total Environment* 473, 422-436 (2014).

[9] D. Melamed, «Monitoring arsenic in the environment: a review of science and technologies with the potential for field measurements,» *Analytica Chimica Acta* 532(1), 1-13 (2005).

[10] J. Ma, M. K. Sengupta, Y. Dongxing and P. K. Dasgupta, «Speciation and detection of arsenic in aqueous sample: A review of recent process in non-atomic spectrometric methods,» *Analytica Chimica Acta* 831, 1-23 (2014).

[11] J. Hao, M.-J. Han, S. Han, X. Meng, T.-L. Su and Q. K. Wang, «SERS detection of arsenic in water: a review,» *Journal of Environnemental Sciences* 36, 152-162 (2015).

[12] https://www.trace2o.com/product-page/arsenometer [Access 27 July 2022].

[13] https://www.metrohm.com/en_gb/products/voltammetry/portable-va-analyser.html [Access 27 july 2022].

[14] https://en.klearia.com/monitoring [access 27 july 2022].

[15] K. Kneipp, H. Kneipp, I. Itzkan, R. R Dasari and M. S Feld, «Surface -enhanced Raman scattering and biophysics,» *J. Phys. Cond. Mat. 14(18),* R597-R624 (2002).

[16] S. Degioanni, A. M. Jurdyc, A. Cheap, B. Champagnon, F. Bessueille, J. Coulm, L. Bois and D. Vouagner, «Surface-enhanced Raman scattering of amorphous silica gel adsorbed on gold substrates for optical fiber sensors,» *Journal of Applied Physics* 118(115), 153103 (2015).

[17] S. J. Greaves and W. P. Griffith, «Surface-enhanced Raman scattering (SERS) from silver colloids of vanadate, phosphate and arsenate,» *Journal of Raman Spectroscopy* 19(18), 503-507 (1988).

[18] R. Liu, J.-f. Sun, D. Cao, L.-q. Zhang, J.-. Liu et G.-B. Jiang, «Fabrication of highly-specific SERS substrates by co-precipitation of functional nanomaterials during the self-sedimentation of silver nanowires into a nanoporous film,» *Chemical Communications* 51(17), 1309-1312 (2015).

[19] J. Hao, M.-J. Han, Z. Xu, J. Li and X. Meng, «Fabrication and evolution of multilayer silver nanofilms for surface-enhanced Raman scattering sensing of arsenate,» *Nanoscale Research Letter* 6(1), 1-11 (2011).

[20] M. Vinod and K. Gopchandran, «Bi-metallic Au-Ag nanochains as SERS substrates,» *Current Applied Physics* 15(8), 857-863 (2015).

[21] H. Tang, C. Zhu, G. Meng and N. Wu, «Review—Surface-enhanced raman scattering sensors for food,» *Journal of The Electrochemical Society* 165(8), B3098-B3118 (2018).

[22] http://gwyddion.net/

[23] D. E. Irish et O. Puzic, «Raman spectral study of the constitution and equilibria of nitric acid and d-nitric acid,» J. *Solution Chem.* 10(6), 377–393 (1981).

[24] A. Ruas, P. Pochon, J.-P. Simonin et P. Moisy, «Nitric acid: modeling osmotic coefficients and acid–base dissociation using the BIMSA theory,» *Dalton Transactions* 39(42), 10148-10153 (2010).

[25] J. J. Mock, M. Barbic, D. R. Smith, D. A. Schultz and S. Schultz, «Shape effects in plasmon resonance of individual colloidal silver nanoparticles,» *The Journal of Chemical Physics* 116(115), 6755-6759 (2002).

[26] K. Chatterjee, S. Banerjee and D. Chakravorty, «Plasmon resonance shifts in oxide-coated silver nanoparticles,» *Physical Review B* 66(8), 085421 2002).

[27] M. D. McMahon, R. Lopez, H. M. Meyer, L. C. Feldman and R. F. Haglund, «Rapid tarnishing of silver nanoparticles in ambient laboratory air,» *Applied Physics B* 80(7), 915-921 (2005).

[28] N. J. Halas, S. Lal, W.-S. Chang, S. Link and P. Nordlander, «Plasmons in strongly coupled metallic nanostructures,» *Chemical Reviews* 111(6), 3913-3961 (2011).

[29] A. Quiroz, R. Sato, E. Massoni, R. Sánchez, G. Bañuelos, N. Sánchez and E. Mata, «Step by step synthesis of silver films by electroless technique and their SERS application of sodium arsenate,» *Materials Research Express,* 6(11), 116439 (2019).

[30] P. K. Jain, W. Huang and M. A. El-Sayed, «On the universal scaling behavior of the distance decay of plasmon coupling in metal nanoparticle pairs: a plasmon ruler equation,» *Nano Letters* 7(7), 2080-2088 (2005).

[31] N. Kalfagiannis, P. Patsalas and D. C. Koutsogeorgis, « Laser annealing as a platform for plasmonic nanostructuring.,» in *Nanoplasmonics - Fundamentals and Applications*, InTech, 2017.

[32] P. J. Jobst, O. Stenzel, M. Schürmann, N. Modsching, S. Yulin, S. Wilbrandt, D. Gäbler, N. Kaiser and A. Tünnermann, «Optical properties of unprotected and protected sputtered silver films: Surface morphology vs. UV/VIS reflectance,» *Advanced Optical Technologies* 3(1), 91-102 (2014).

[33] K. Seal, D. A. Genov, A. K. Sarychev, H. Noh, V. M. Shalaev, Z. C. Ying, X. Zhang and H. Cao, «Coexistence of localized and delocalized surface plasmon modes in percolating metal films,» *Physical Review Letters* 97(20), 206103 (2006).

[34] A. Merlen and F. Lagugné-Labarthet, «Imaging the optical near field in plasmonic nanostructures,» *Applied Spectroscopy* 68(12), 1307-1326 (2014).

[35] S. Smitha, K. Nissamudeen, D. Philip and K. Gopchandran, «Studies on surface plasmon resonance and photoluminescence of silver nanoparticles,» *Spectrochimica Acta Part A: Molecular and Biomolecular Spectroscopy* 71(1), 186-190 (2008).

[36] G.-N. Xiao and M. Shi-Qing, «Surface-enhanced Raman scattering of methylene blue absorbed on cap-shaped silver nanoparticles,» *Chemical Physics Letters* 447(4-6), 305-309 (2007).

[37] R. R. Naujok, R. V. Duevel and R. M. Corn, «Fluorescence and fourier transform surface-enhanced Raman scattering measurements of methylene blue adsorbed onto a sulfur-modified gold electrode,» *Langmuir* 9(7), 1771-1774 (1993).

[38] U. Laor and C. Schartz, «The role of surface roughness in surface enhanced raman spectroscopy (SERS) the importance of multiple plasmon resonances,» *Chemical Physics Letters* 82(3), 566-570 (1981).

[39] I. Pockrand, «Surface-enhanced Raman scattering from evaporated Ag films : size of revelant roughness features and range of classical enhancement,» *Chemical Physics Letters* 92(5), 509-513 (1982).

[40] J. Rodriguez-Fernandez, A. M. Funston, J. Perez-Juste, R. A. Alvarez-Puebla, L. M. Liz-Marzan and P. Mulvaney, «The effect of surface roughness on the plasmonic response of individual sub-micron gold sphere,» *Physical Chemistry Chemical Physics* 11(28), 5909-5914 (2009).

[41] A. G. Brolo, D. E. Irish, B. D. Smith, « Applications of surface enhanced Raman scattering to the study of metal-adsorbate interactions », *J. Molecular Structure* 405(1), 29-44 (1997).

[42] W.-X. Chen, H. Jiang, Z.-D. Xu and Y. Lu, «Study on the chemisorption kinetics of methylene blue using SERS technique,» *Chinese Journal of Chemistry* 17(2), 125-131 (1999).

[43] M. Sackmann and A. Materny, «Surface enhanced Raman scattering (SERS) a quantitative analytical tool?,» *Journal of Raman Spectroscopy* 37(1-3), 305-310 (2006).

[44] L. Zhong, Y. Hu and D. Xing, «Adsorption orientation of methylene blue (MB+) on the silver colloid: SERS and DFT studies,» *in Conference on Lasers and Electro-Optics/Pacific Rim 2009*, (Optica Publishing Group, 2009), paper TUP14_1.

[45] Z. Li , C.-J. Wang and W.-T. Jiang, "Intercalation of Methylene Blue in a High-Charge Calcium Montmorillonite — An Indication of Surface Charge Determination," *Adsorption Science & Technology,* 28(4) 297-312 (2010).

[46] M. Mulvihill, A. Tao, K. Benjauthrit, J. Arnold and P. Yang, «Surface-enhanced Raman spectroscopy for trace arsenic detection in contaminated water,» *Angewandte Chemie International Edition* 47(34), pp. 6556 –6560 (2008).

[47] M. C. Teixeira and V. S. T. Ciminelli, «Development of a biosorbent for arsenite: Structural modeling based on X-ray spectroscopy,» *Environmental Science & Technology* 39(3), 895-900 (2005).

[48] C. Han, H. Li, H. Pu, H. Yu, L. Deng, S. Huang and Y. Luo, «Synthesis and characterization of mesoporous alumina and their performances for removing arsenic (V),» *Chemical Engineering Journal* 217, 1-9 (2013).

[49] G. Jha, S. Mukhopadhyay, A. L. Ulery, K. Lombard, S. Chakraborty, D. C. Weindorf, D. VanLeeuwen and C. Brungard, «Agricultural soils of the Animas River watershed after the Gold King Mine spill: An elemental spatiotemporal analysis via portable X-ray fluorescence spectroscopy,» *Journal of Environmental Quality* 50(3), 730-743 (2021).

AIP Publishing

Journal of Applied Physics

ACCEPTED MANUSCRIPT

This is the author's peer reviewed, accepted manuscript. However, the online version of record will be different from this version once it has been copyedited and typeset.
PLEASE CITE THIS ARTICLE AS DOI: 10.1063/5.0126372

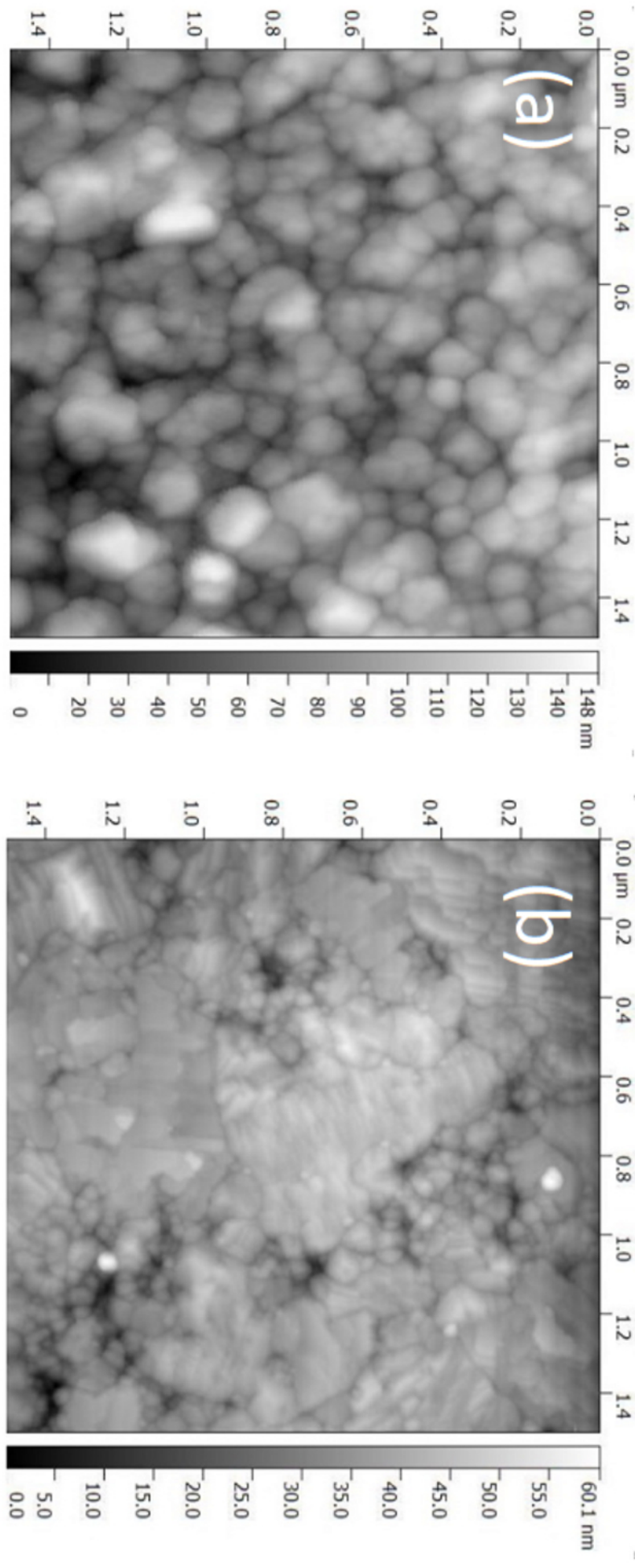

AIP Publishing

Journal of Applied Physics

ACCEPTED MANUSCRIPT

This is the author's peer reviewed, accepted manuscript. However, the online version of record will be different from this version once it has been copyedited and typeset.
PLEASE CITE THIS ARTICLE AS DOI: 10.1063/5.0126372

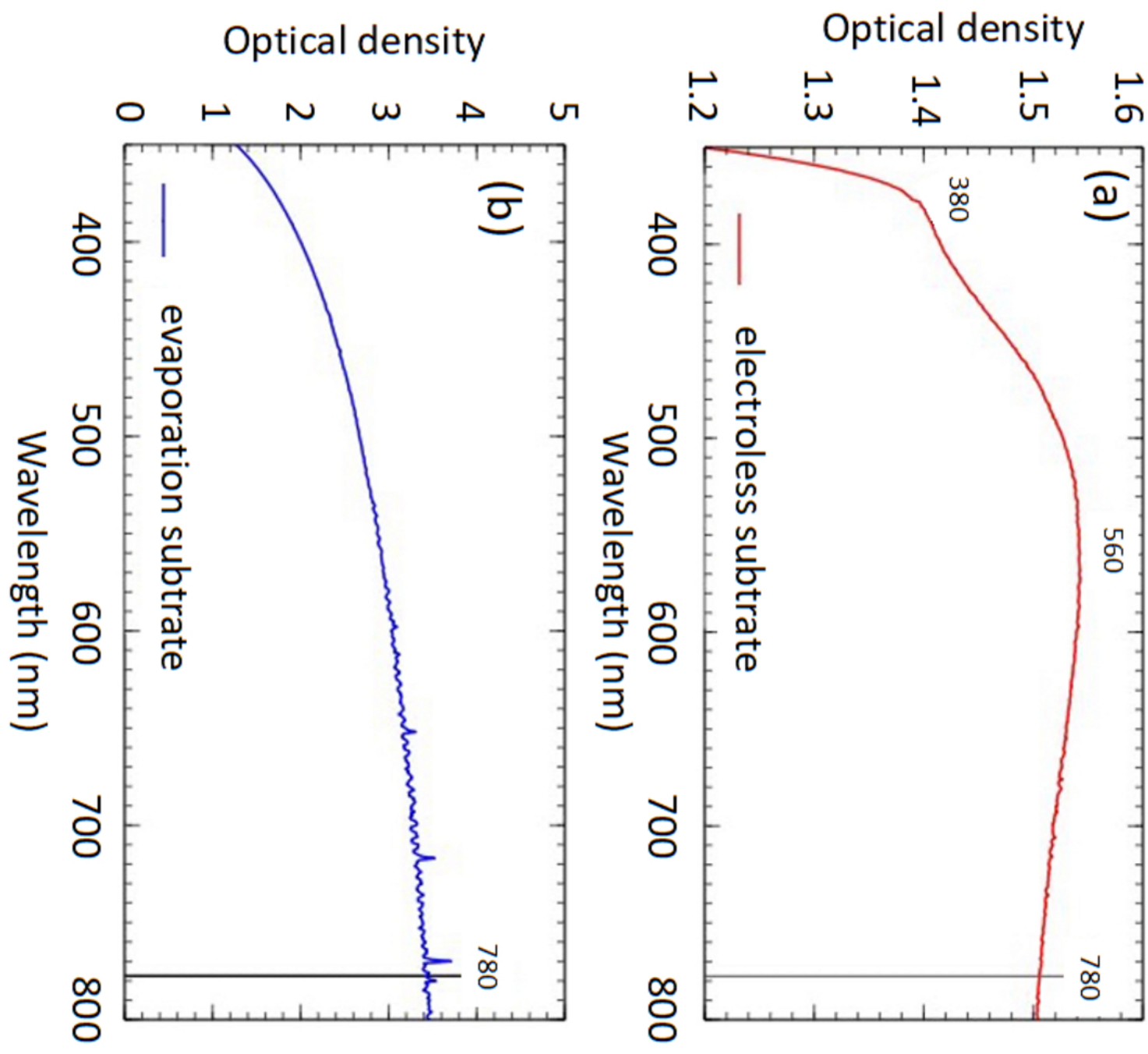

Journal of Applied Physics